

NeuroLGP-SM: Scalable Surrogate-Assisted Neuroevolution for Deep Neural Networks

Fergal Stapleton*

Naturally Inspired Computation Research Group,
Department of Computer Science, Hamilton Institute
Maynooth University, Ireland
fergal.stapleton.2020@mumail.ie

Edgar Galván*

Naturally Inspired Computation Research Group,
Department of Computer Science, Hamilton Institute
Maynooth University, Lero, Ireland
edgar.galvan@mu.ie

Abstract—Evolutionary Algorithms (EAs) play a crucial role in the architectural configuration and training of Artificial Deep Neural Networks (DNNs), a process known as neuroevolution. However, neuroevolution is hindered by its inherent computational expense, requiring multiple generations, a large population, and numerous epochs. The most computationally intensive aspect lies in evaluating the fitness function of a single candidate solution. To address this challenge, we employ Surrogate-assisted EAs (SAEAs). While a few SAEAs approaches have been proposed in neuroevolution, none have been applied to truly large DNNs due to issues like intractable information usage. In this work, drawing inspiration from Genetic Programming semantics, we use phenotypic distance vectors, outputted from DNNs, alongside Kriging Partial Least Squares (KPLS), an approach that is effective in handling these large vectors, making them suitable for search. Our proposed approach, named Neuro-Linear Genetic Programming surrogate model (NeuroLGP-SM), efficiently and accurately estimates DNN fitness without the need for complete evaluations. NeuroLGP-SM demonstrates competitive or superior results compared to 12 other methods, including NeuroLGP without SM, convolutional neural networks, support vector machines, and autoencoders. Additionally, it is worth noting that NeuroLGP-SM is 25% more energy-efficient than its NeuroLGP counterpart. This efficiency advantage adds to the overall appeal of our proposed NeuroLGP-SM in optimising the configuration of large DNNs.

Index Terms—Neuroevolution, Linear Genetic Programming, Surrogate-assisted Evolutionary Algorithms

I. INTRODUCTION

Evolutionary Algorithms (EAs) [10] have proven to be effective in both the crafting of architectures and hyperparameter optimisation of Deep Neural Networks (DNNs) [25]. This application is commonly known as neuroevolution [11], and have been applied to numerous problem domains, such as autonomous vehicles [14], [39] and face recognition [8], [9]. The pursuit of optimal DNN architectures has led to various methodologies, including EAs [11], reinforcement learning [44], etc. However, a significant challenge persists across these methods: the substantial computational resources required to identify high-performing networks.

The rise of GPU-accelerated hardware has helped alleviate some of this computational cost, however, a significant proportion of research in DNNs is based on incremental improvements on DNN algorithms for benchmark problems, where

there is a significant correlation between network complexity for incremental gains in terms of additional performance. In fact, when looking at very large models of hundreds of billions of parameters, it can cost millions of dollars for a single iteration [26]. This energy consumption is further compounded when considering population-based neuroevolutionary techniques which require many networks to be trained and evaluated in order to find suitable architectures.

One way to address this significant issue is with the use of surrogate-assisted evolutionary algorithms (SAEAs). SAEAs can be used to estimate the fitness of DNNs without the need to fully train each network. In particular, surrogate modelling strategies that employ Bayesian optimisation have shown much promise [26]. However, a major challenge remains in how best to deal with the surrogate representation. For instance, using genotype information to build surrogates often requires complex encoding strategies [41], and in some instances, constructing adequate distance metrics to compare different network topologies is not feasible [40]. Using phenotypic information on the other hand has shown some promise [19], [40], but a challenge remains in scaling to deeper and more complex networks which inherently requires a high-dimensional representation [38].

In this work, we analyse a novel population-based Neuroevolutionary technique, referred to as NeuroLGP, and its surrogate model variant NeuroLGP-SM [36]. Using a robust model management strategy, we use phenotypic distance vectors to estimate the performance of partially trained DNNs. These vectors are comparatively large for the optimisation problem at hand [38] and, as such, we use an approach that is designed for handling high-dimensional data, known as Kriging Partial Least Squares (KPLS). This approach allows for a novel and scalable surrogate-assisted technique that is skilfully adept at handling neuroevolution of DNNs and to the the best of our knowledge, this method of surrogate-assisted neuroevolution has not been studied before.

The aim of this study is to apply Surrogate-assisted Evolutionary Algorithms (SAEA) in neuroevolution, using Kriging Partial Least Squares (KPLS) on phenotypic distance vectors inspired by Genetic Programming Semantics. Our key contributions are outlined as follows, 1) **Efficient Fitness Estimation:** We demonstrate the accurate estimation of DNN fitness

*joint-first authorship

values without full evaluations through our proposed approach, NeuroLGP-SM, employing KPLS on phenotypic distance vectors. 2) **Performance Metrics:** We employ three well-defined metrics to assess the predictive capabilities of NeuroLGP-SM in terms of model fitness. These results align with the competitive or superior performance of our NeuroLGP-SM approach compared to 12 popular techniques, including convolutional neural networks, autoencoders, and support vector machines, across four challenging classification tasks. 3) **Energy Consumption Analysis:** We provide a reliable formula to gauge the energy consumption of our approaches, revealing that NeuroLGP-SM is 25% more efficient compared to its counterpart that does not use surrogate models and 4) **Encoding for Analysis:** Through clever encoding, we allow easy access to analyse the internal structures of the architectures, enabling us to conduct an in-depth analysis of the networks discovered by our proposed approaches.

II. RELATED WORK

A. Neuroevolution using Surrogate Models

Santos et al. [33] proposed a novel approach that makes use of semantics in neuroevolution. They do so by using Geometric Semantic Genetic Programming, in conjunction with a neuroevolutionary approach called Semantic Learning Machines (SLM) [16], a form of neuroevolution technique. Furthermore, Hagg et al. [19], made the connection between semantic distances in GP and phenotypic distances within the context of surrogate-assisted evolutionary algorithms for neuroevolution. Similarly, Stork et al. [40] extended CGP to use a surrogate-assisted neuroevolution approach that makes use of phenotypic distance vectors. A limitation of Stork’s work is the scalability of using Kriging on high-dimensional data. For instance, in the recent work by Stapleton and Galván, highlighted that traditional approaches such as the Kriging approach suffer with high-dimensionality [38] and may not be suitable for DNN architectures.

Freeze-Thaw Bayesian Optimisation (FBO), proposed by Swersky et al. [43], uses Bayesian optimisation to determine whether a particular neural network that has been partially trained should be fully evaluated. This approach is novel in that the system stops training (or freezing) of less promising networks, instead spending valuable resources on the most promising networks. Of note, is the fact that the FBO approach relies on the phenotypic behaviour of DNNs. It is important to note the majority of works rely on genotypic information when building surrogate models for neuroevolution [17], [41]. For reference, a major work in this regard is that of Sun et al. [41] referred to as the End-to-End Performance Predictor. This approach uses an offline surrogate model based on random forests to accelerate learning of CNN architectures. The CNN architecture is encoded such that it maps to a numerical decision variable, which is passed to the random forest-based surrogate-model. Not only does this approach not require large amounts of training time but, also alleviates the requirement of a smooth learning curve [43].

III. BACKGROUND

A. Surrogate assisted models: Kriging and Kriging Partial Least Squares

Surrogate modelling has many use cases but in the context of this work, the aim is to effectively estimate the fitness values for candidate solutions while simultaneously reducing the run time of the evolutionary process. To this end, not only must the surrogate model be well-posed, but also, the evolutionary process must interact with a robust surrogate model management strategy [20]. The surrogate model differs from the parent model that instead of training directly on the data the surrogate model is trained on the design space, where the aim is to identify and further explore regions of this design space that will produce preferable parameters. As such, interpolation-based approaches may be used to simulate the unknown regions of the parameter space, such as Gaussian processes, commonly referred to as Kriging. Another benefit to the Kriging approach is that it allows for estimates of the uncertainty of predictions.

Kriging is an interpolation-based technique that assumes spatial correlation exists between known data points, based on the distance, and variation between these points. We aim to use observations $\{y(x_1), y(x_2), \dots, y(x_n)\}$ to help estimate an unknown function value $\hat{y}(x^*)$ for the unknown data point x^* , where n is the number of individuals in the training data. A kernel function $K(\cdot)$ is used to express the spatial correlation between two samples x_i and x'_i as shown in Eq. 1,

$$k(x, x') = \prod_{i=1}^m \exp(-\theta(\mathcal{D}(x_i, x'_i))) \quad (1)$$

where the θ parameter controls the rate at which the correlation decays to zero between x_i and x'_i and $\mathcal{D}(x_i, x'_i) = (x_i - x'_i)^2$. The θ parameter is determined using the Maximum Likelihood Estimator (MLE). A significant drawback, however, is that for large dimensions m , the computational cost increases dramatically since the MLE algorithm calculates the inverse of the correlation matrix multiple times.

Kriging Partial Least Squares (KPLS) helps to alleviate this limitation by reducing the number of parameters calculated [4]. It does so by using partial least squares which project the high-dimensional data into a lower dimension using principal components. Eq. 2 details the KPLS kernel,

$$K(x, x') = \prod_{k=1}^h \prod_{i=1}^m \exp(-\theta_k(w_i^{(k)} x_i - w_i^{(k)} x'_i)^2) \quad (2)$$

where w are rotated principal directions which maximise the covariance and are a measure of how important each principal component is. Typically, the number of principal components h is much less than the number of dimensions m and, as such, allows for the substantial improvement in computational cost associated with the KPLS approach. See [4] for details.

B. Phenotypic Distance

The inspiration for using phenotypic distance is by works such as Stork et al. [40] and Galván et al. [12], [13], [15], [37], whose previous work in GP centred on semantics, in particular, the use of semantic distance metrics. In traditional GP, semantics can be understood as the behaviour of program given a finite set of inputs. A definition by Pawlak et al. [31] states

Def 1. *The semantics $s(p)$ of a program p is the vector of values from the output set O obtained by computing p on all inputs from the input set I . This is expressed in Eq. 3,*

$$s(p) = [p(in_1), p(in_2), \dots, p(in_l)] \quad (3)$$

where $l = |I|$ is the size of the input set and where the inputs in from can be some subset of the dataset. In terms of neuroevolution, we can define a solution sample x as having the semantic or phenotypic behaviour of the i^{th} program such that $x_i = s(p_i)$, where the semantics $s(p)$ is the vector of values from the output. From Eq. 1 we can then define our phenotypic distance \mathcal{D} as,

$$\mathcal{D}(x_i, x_j) = \mathcal{D}(s(p_i), s(p_j)) \quad (4)$$

As such the distance metric is dependent on the outputs of each network, where the x_i is a flattened vector containing the outputs from the final layer for all data instances. This phenotypic distance vector length, as such, is the number of images of the test dataset times the number of classes. Notably, this approach can be extended to any deep learning model architecture that uses a vectorised output (i.e., transformers), however, the limitations and scalability of other deep learning models with this method are yet to be investigated.

IV. METHODOLOGY

A. NeuroLGP

The original Linear Genetic Programming (LGP) encoding is based on the concept of using registers, which are units computer memory storage for manipulating data while executing instructions, in a low-level programming context. The content of these registers are altered using instruction operations. There are three main components to instruction; an *operand* which performs a specific function on one or more *registers* which store the result in a *destination register*. In the case of 2-register instruction encoding the operand operates on a single instruction and for a 3-register instruction encoding operates on two instructions. The left of Fig. 1 highlights an example of LGP written in C code, where $r[i]$ denotes the i^{th} register. This example contains both effective and non-effective lines of code, where the non-effective lines of code are commented out and subsequently not compiled. Each line of code is executed imperatively. The register $r[0]$ is a specially designated register for the final output of the program. With the NeuroLGP approach, instead of using registers to store small amounts of data, we instead use the idea of registers as pointers to much larger amounts of data.

<pre>void gp(r) double r[8]; { ... r[0] = r[5] + 71; // r[7] = r[0] - 59; if (r[1] > 0) if (r[5] > 2) r[4] = r[2] * r[1]; // r[2] = r[5] + r[4]; r[6] = r[4] * 13; r[0] = r[6]; }</pre>	<pre>def neuro_gp(...) { ... r[0] := Conv(r[1]) // r[4] := MaxPool(r[3]) // r[7] := Conv(r[4]) r[5] := MaxPool(r[2]) r[6] := Conv(r[5]) r[3] := AvgPool(r[6]) // r[5] := MaxPool(r[8]) r[0] := Dense(r[3]) }</pre>
---	--

Fig. 1: *left*: LGP example in C language. Based on example from [5]. *right*: NeuroLGP pseudocode for python.

As such, the registers instead control the flow of the initial and intermediary data from each outputted layer of our evolvable DNN. The right of Fig. 1, demonstrates how the expected representation would look, where the general form of this code is similar to the figure on the left.

Traditionally, in LGP, registers can be of different types (input registers, calculation registers and constant registers). In this work, each register is initialised with the inputs of various layers within the neural network and so act as just input registers (though it may be useful to have special registers specifically for handling skip connections and multiple branches). While this may seem wasteful in terms of memory, multiple registers are only used in the genotypic representation and when calculating the fitness, the number of effective registers can be reduced as part of a repair process. Likewise, the non-effective code can also be removed at the same time. As such, the phenotypic representation of the network will not only be much simpler than the genotypic representation, but also much smaller. Fig.2 demonstrates the genotype-to-phenotype mapping.

B. NeuroLGP with Surrogate Model (NeuroLGP-SM)

To identify individuals requiring full evaluation, we use the Expected Improvement (EI) criteria [21]. EI guides the selection of candidate solutions for evaluation by estimating the improvement over the current best solution. This enables us to prioritise solutions from areas in the search space expected to exhibit the most significant improvement. The calculation of EI is shown in Eq. 5,

$$EI = \begin{cases} (\hat{f}(x) - f(x^*))\Phi(Z) + \sigma(x)\phi(Z) & \text{if } \sigma(x) > 0 \\ 0 & \text{if } \sigma(x) = 0 \end{cases} \quad (5)$$

$$Z = \frac{\hat{f}(x) - f(x^*)}{\sigma(x)}$$

where $\hat{f}(x)$ is the model's predicted performance of the surrogate for the phenotypic distance vector x , where $f(x^*)$ is the best-known value of the objective function so far (in this case maximum) and Φ and ϕ are the cumulative distribution function (CDF) and probability density function (PDF) of the standard normal distribution, respectively. Fig. 3

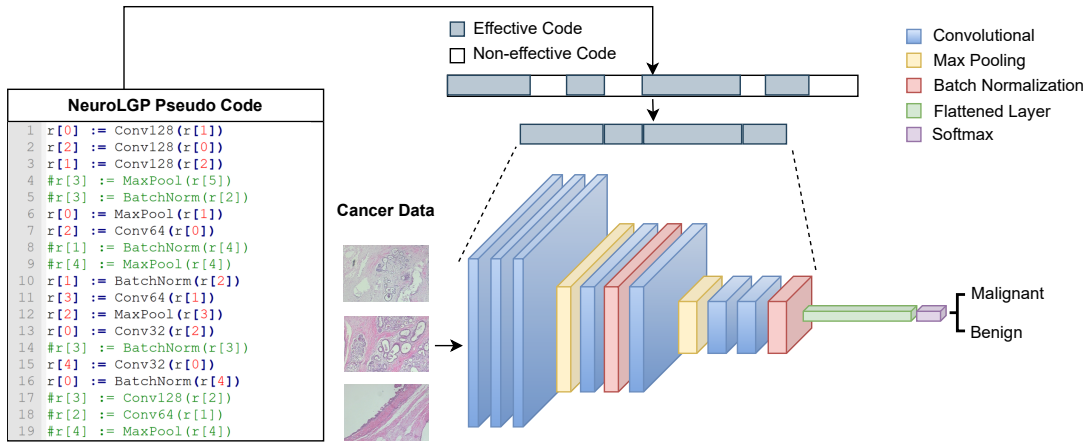


Fig. 2: Diagram of the NeuroLGP genotype-to-phenotype mapping. The pseudocode for the set of instructions (left-hand side) can be represented as the genotype with effective and non-effective code (top) and produces the resulting phenotype (bottom right-hand side) as a specific neural network architecture. Note that the non-effective coding is not present in the phenotype.

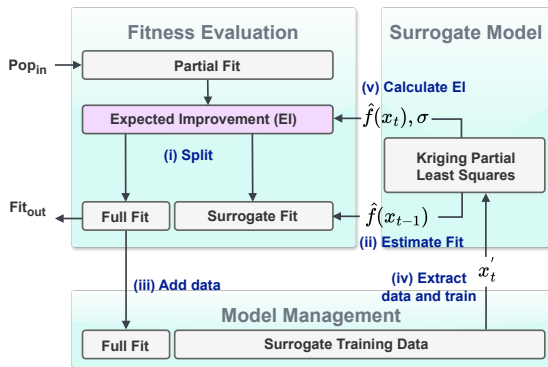


Fig. 3: Model management strategy in terms of fitness evaluation, model management and training the surrogate model.

summarises the surrogate model management strategy. The annotations are: (i) *Split*: first, the population is split with a 40/60 split for individuals to be fully evaluated vs. the partially trained individuals, respectively, (ii) *Estimate fitness*: the fitness is estimated using the KPLS approach as informed by the previous generation, (iii) *Add data*: the phenotypic distance vector for the fully evaluated portion of the population is added to the surrogate training data (note: the phenotypic distance vector is taken before the full fitness evaluation), (iv) *Extract data and train*: the phenotypic distance vectors are collectively used to train the KPLS approach as detailed in Section III-A, and (v) *Calculate EI*: the EI criteria is calculated for the incoming population of individuals.

V. EXPERIMENTAL SETUP

The Breast Cancer Histopathological Image Classification (BreakHis) [35] is a binary classification dataset consisting of microscopic images containing 2,480 benign and 5,429 malignant tumours, where images were obtained as four different magnifications ($\times 40$, $\times 100$, $\times 200$ and $\times 400$) and are split into

four individual datasets for this work. Each image consists of 64×64 pixels (down-scaled resolution from 700×460 pixels) and 3-channel RGB with 8-bit depth in each channel. The split for training, validation, test and test2 is approximately (63.5%, 12.5%, 12.5%, 12.5%), where the first three splits conform to a ratio of (70:15:15), conforming to the general training/test split as seen in other approaches (Table I). The first three splits are used purely for training and evaluating networks and the last split is retained for an unbiased analysis of the evolutionary process. The dataset is imbalanced and the synthetic minority oversampling technique [6] is used to up-sample the minority class.

We employ two approaches to investigate the validity and quality of our proposed surrogate-assisted neuroevolution model. These are: (i) The *NeuroLGP* approach, which uses a novel encoding to evolve the structure of our networks, training to the full number of epochs as outlined in Section IV-A, and (ii) The *NeuroLGP-SM* approach where we integrate the surrogate modelling strategy, as outlined in Section IV-B, into the *NeuroLGP* approach. Experiments were conducted using Kay supercomputer provided by the Irish Centre for High-End Computing (ICHEC). Experiments were run in parallel, with each run assigned to a single Nvidia Tesla V100 GPU with 16GB Ram. Additionally, each run has access to a 20-core 2.4 GHz Intel Xeon Gold 6148 (Skylake) CPU processor which is used during training of the surrogate model portion of the NeuroLGP-SM approach. Overall, the NeuroLGP approach took ~ 28 GPU days and the NeuroLGP-SM approach ~ 21 GPU days, for 8 runs across the 4 datasets.

VI. RESULTS

A. Comparison of Models

Table I summarises approaches that have used the BreakHis data set from the last few years, including our proposed approaches. Most of these works have been taken from a comprehensive 2020 review paper from Benhammou et al. [3].

For fair comparison, we have selected works that also do not use transfer learning as these represent manually crafted networks that have zero pre-training. Furthermore, many of these approaches use specialised feature extraction and pre-processing steps for histopathological data. As such, our goal is not necessarily to outperform previous state-of-the-art works, but rather to show that our neuroevolutionary technique can achieve similar results to hand-crafted architectures, even without specialised knowledge of the problem domain.

Looking at the last four columns from the right, we list the accuracies for the various magnifications. The last four rows correspond to our proposed approaches: NeuroLGP and its surrogate-assisted variant (NeuroLGP-SM). We can see that our results are in good accordance with the other works, in some cases outperforming other approaches. Notably, the results yielded by our two approaches on the $\times 200$ magnification are very competitive in terms of accuracy.

If we turn our attention to specifically comparing the NeuroLGP-SM and NeuroLGP models, we can see that each has very similar performances. For instance, the mean values (third and fourth last lines from bottom), the NeuroLGP-SM and NeuroLGP models are typically within 0.2% of each other and for the best (last two lines) the NeuroLGP-SM and NeuroLGP models are within 1-2%.

B. Analysis of the NeuroLGP-SM Model

Three metrics are used to determine how well the surrogate model performs in predicting the fitness of our partially trained models: (i) the Mean Squared Error (MSE) gives a measure of how accurate our model is in terms of predicting fitness where values close to 0 are preferable, (ii) Kendall’s Tau is used to measure the correlation between the predicted fitness and the actual fitness [42], where values close to 0 indicates no correlation, -1 a perfect negative correlation, +1 a perfect positive correlation, and (iii) the R^2 score is a measure of how close the predicted value is to its true value and ranges from $-\infty$ to 1 and explains how much variability is in the prediction model, where values closer to 1 are preferable.

Table II summarises the effectiveness of the NeuroLGP-SM model for each of the datasets. The low MSE values, as seen in the first row, show a relatively low error between the predicted and actual fitness across the four dataset. The Kendall’s Tau values range from 0.5647 to 0.6791, indicating a strong positive correlation between the actual and predicted fitness. We can see that for $\times 40$ we have R^2 of 0.5026 indicating a moderate level of fit being captured by the surrogate model while for $\times 100$, $\times 200$ and $\times 400$, we have R^2 values of 0.6665, 0.7079 and 0.7786. There is also a general trend showing the R^2 score increasing with higher magnifications. This may be a result of more noise/artefacts present in the lower magnification images, making it more difficult for the surrogate model to predict based on the network outputs but further studies would be required to confirm this. Overall, the quality of fit and performance of the surrogate models based on the three metrics is very strong for each dataset.

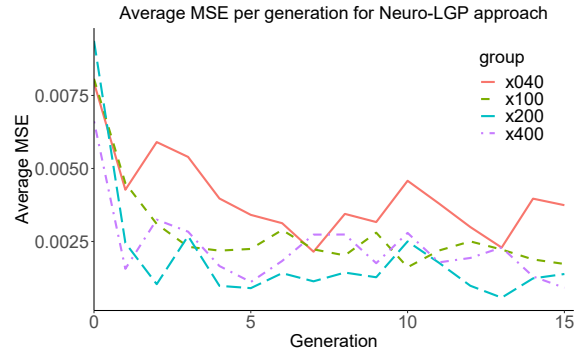


Fig. 4: Avg. MSE between predicted vs. actual fitness over 15 generations for the NeuroLGP-SM approach. The relative stability shows the robustness of the NeuroLGP-SM approach.

Next, we plot the average MSE per generation to get an idea of how the predictive capability of the NeuroLGP-SM approach changes over time as seen in Fig. 4. MSE values that either decrease or remain stable are preferable, as increasing MSE values would indicate our surrogate model is losing its predictive capability as new individuals are introduced. We can see that after an initial drop in average MSE from the first couple of generations (x-axis), while there are some fluctuations in the average MSE, in general values remain relatively stable, demonstrating the robustness of our NeuroLGP-SM.

Fig. 5 details the quality of fit in terms of how well the predicted accuracies relate to the actual accuracies. In each figure, values closer to the red diagonal line, represent individuals that have a better quality of fit. We can see that the higher the accuracy the closer our predicted values are to the red line. This is a by-product of the surrogate model management strategy we employ. In essence, we are less concerned with the accuracies of poorer-performing models, instead, we have taken a more greedy approach favouring models that are better performing.

Figure 5a informs us why the $\times 40$ magnification slightly under-performed in terms of the metrics as shown in Table II. We can see that for the predicted values, on the y-axis, there are quite several individuals predicted to have 80% accuracy when the actual accuracies, for these individuals range from 30-80% in terms of actual accuracy, as shown on the x-axis. A deeper dive revealed that this was a result of one particularly bad-performing run and was not present in the other 7 runs.

C. Analysis of the Energy Consumption

We perform a comparison of the estimated energy consumption of the NeuroLGP-SM and the NeuroLGP models using the Green-algorithm by Lannelongue et al. [24]. Eq. 6 is used to get this estimate,

$$E = r_t * (P_c * U + P_m) * PUE * PSF \quad (6)$$

where E is the energy consumed in KW/h, r_t is the runtime, P_c is the power draw for the computing cores and depends on the CPU/GPU model, U is the usage factor, P_m is the power

TABLE I: Accuracy results for approaches using BreakHis dataset ($\times 40$, $\times 100$, $\times 200$ and $\times 400$). Results from this work are highlighted in boldface and are presented in the last four rows. WSI: wholes slide image, CNN: convolutional neural network, SVM: support vector machine, AE: auto-encoder, DBN: deep-belief network.

Work	Preprocessing	Patch/slide	Model	Training/Test	$\times 40$	$\times 100$	$\times 200$	$\times 400$
Gupta [18]	None	WSI	Ensemble	70% / 30%	88.9	88.9	88.9	88.9
Sharma [34]	Mixed	WSI	Ensemble	Not specified	81.7 ± 2.8	81.2 ± 2.7	80.7 ± 3.4	81.5 ± 3.1
Nahid [27]	None	WSI	CNN	Not specified	94.4	95.93	97.19	96
Nahid [28]	K-Mean Clustering	WSI	CNN	Not specified	85	90	90	90
Karthiga [22]	K-Mean Clustering	WSI	SVM	Not specified	93.3	93.3	93.3	93.3
Pratiher [32]	Gray Scale, Data Aug	WSI	AE	Not specified	96.8	98.1	98.2	97.6
Badejo [2]	None	WSI	SVM	70% / 30%	91.1	90.7	86.2	84.3
Nahid [29]	Contrast Enhancement	WSI	DBN	70% / 30%	88.7	89.06	88.84	87.67
Das [7]	Resize (370x230)	Patches (224x224)	CNN	80% / 20%	89.52	85.3	88.6	88.4
Kumar [23]	Stain Normalisation	Patches (64x64, 32x32)	CNN	70% / 30%	82 ± 2.8	86.2 ± 4.6	84.6 ± 3.0	84 ± 4.0
Aswathy [1]	Mixed	WSI	SVM	90% / 10%	89.1	89.1	89.1	89.1
NeuroLGP (Mean)	Resize (64x64), Data Aug	WSI	CNN	See Section V	89.7 ± 2.1	0.872 ± 3.0	92.6 ± 2.1	90.8 ± 1.0
NeuroLGP-SM (Mean)	Resize (64x64), Data Aug	WSI	CNN	See Section V	89.8 ± 1.4	0.873 ± 1.8	92.8 ± 2.4	91.0 ± 0.7
NeuroLGP (Best)	Resize (64x64), Data Aug	WSI	CNN	See Section V	93	91.6	96	92.5
NeuroLGP-SM (Best)	Resize (64x64), Data Aug	WSI	CNN	See Section V	91.3	90.3	97	92.5

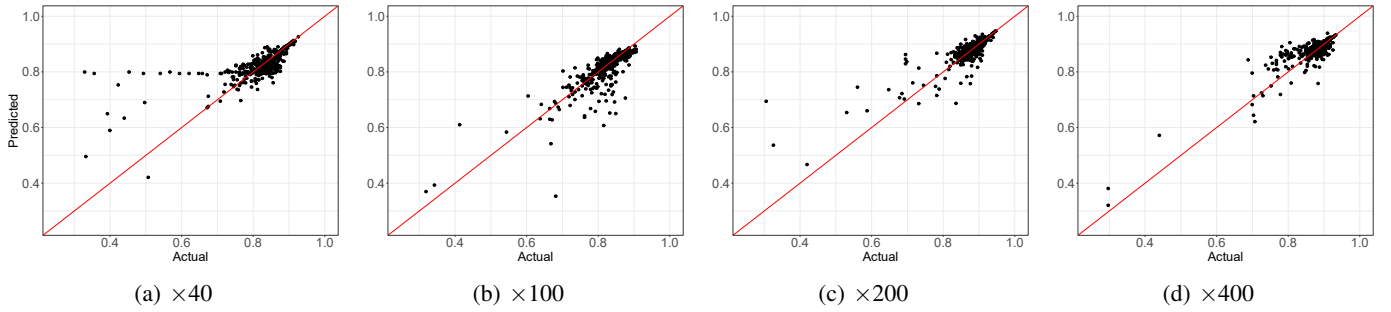


Fig. 5: Predicted vs. actual accuracies (black points), for $\times 40$, $\times 100$, $\times 200$, and $\times 400$ datasets, shown in (a) – (d), respectively, across 8 independent runs for the surrogate-assisted approach (NeuroLGP-SM). The red line denotes where the accuracy for both predicted and actual are the same, where points closer to this line are preferential.

TABLE II: Average MSE, Kendall’s Tau and R^2 .

Metric	Magnification Size			
	$\times 40$	$\times 100$	$\times 200$	$\times 400$
MSE	0.0037	0.0017	0.0014	0.0009
Kendall’s Tau	0.6019	0.6791	0.6225	0.5647
R^2	0.5026	0.6665	0.7079	0.7786

draw for the memory. *PUE* is the Power Usage Efficiency and is a measure of how much additional energy is needed to operate the data centre. *PSF* is the Pragmatic Scaling Factor and can be used to estimate the performance when multiple runs are taken into consideration. A conservative *PUE* value of 1.67 was used, which represents the worldwide average power usage *PUE* across all data centres [24]. For simplicity, *PSF* was kept as 1 as we are interested in the average runtime rather than the cumulative runtime.

The real usage factor was minimal for both the NeuroLGP-SM and the NeuroLGP models, even during training for the NeuroLGP-SM model and additionally, the CPU energy consumption is negligible compared to that of the GPU, so we have reported just the energy saved by the GPU, overall 2.79 KW/h are saved using the NeuroLGP-SM model. Considering the total energy saved across all 4 magnifications for 8 runs each, we save approximately 89.28 KW/h: 25% less energy is consumed using the NeuroLGP-SM approach.

D. Analysis of Genotype

Figs. 6 (a) and (b) show the proportions of various genes for two of the four magnifications $\times 100$ and $\times 400$, respectively. Due to page constraints, we have shown only these two datasets, but our analysis for the same for the other two, unless stated otherwise in the text. Initial proportions (blue) represent the proportions of specific genes at initialisation (first generation). The NeuroLGP-SM (green) and NeuroLGP (orange) model are also represented and denote the proportions in the final generation across all 8 runs. The comparison we make will aim to show how the proportions the NeuroLGP-SM and NeuroLGP for specific layers change from initialisation (i.e., we compare green and orange proportions against blue).

For the initial proportions, genes were proportioned based on their functional grouping. The four groups are dropout, batch normalisation, pooling, and convolutional layers. As such, each group makes up a quarter of the initial population and are subsequently divided again by specific genes. For instance, as there are 6 convolutional layer genes we divide $\frac{0.25}{6}$ to get the proportion for each convolutional layer.

Turning our attention to the NeuroLGP-SM and NeuroLGP model, we can see general trends in how the various gene groupings change by the final generation shown in green and orange for the NeuroLGP-SM and NeuroLGP, respectively. For instance, the dropout layer proportions sizes tend to

decrease significantly by the final generation in the NeuroLGP-SM and NeuroLGP models. Similarly, the proportion of batch normalisation layers tends to increase. The pooling layers are more specific to the dataset. For instance, for $\times 100$ there is an increase specifically for the max pooling layer (also found in $\times 200$ but not shown). On the other hand, for $\times 400$ there is a general decrease, albeit the two models differ on the specific pooling layer they decrease. Again, for the convolutional layers there is a more specific trend for particular datasets. While there are some slight increases and decreases in proportion size for $\times 40$, $\times 100$ and $\times 200$, for $\times 400$ there are notable increases in proportion sizes for $\times 400$ for convolutional layers using a 3×3 filter (Figure 6b, CONV_32_3x3, CONV_64_3x3 and CONV_128_3x3).

Some of these trends are unsurprising, we would expect that the proportion of dropout layers would be less, for instance, as CNN architectures are not as prone to overfitting [30]. It would seem that the decrease in pooling layers in the $\times 400$ is being compensated by an increase in convolutional layers, in other words, some of the dimension reduction is being handled by the convolutional layers rather than the pooling. Further research could investigate how these proportions change relative to different resolution sizes. Interestingly, while in many cases the change in proportions are consistent for both the NeuroLGP-SM and NeuroLGP, in some instances the proportion sizes differ significantly, for instance, CONV_64_5x5 as seen in $\times 400$. This is likely a result of solutions converging at different local optima, however, further analysis of the fitness landscape would be beneficial in gaining more insight.

E. Limitations of our analysis

While a single run is the norm in terms of neuroevolution, we endeavoured to perform as many runs as possible, to add better confidence to our analysis. While we ran individual runs in parallel, both the NeuroLGP-SM and NeuroLGP approaches, for 8 runs each and for the 4 datasets, the total runtime amassed ~ 50 GPU days. To conduct a full statistical analysis we would require another +50 GPU days of experimentation. Future work, could look into using different problem domains and different Deep learning models.

VII. CONCLUSION

In this work, we demonstrate a novel surrogate-assisted neuroevolutionary approach, named Neuro-Linear Genetic Programming LGP surrogate model (NeuroLGP-SM). This approach makes use of Kriging Partial Least Squares (KPLS) to estimate the fitness of partially trained Deep Neural Networks (DNNs) using phenotypic distance vectors in a high-dimensional context. This scalable approach to surrogate-assisted neuroevolution is adept at finding robust and efficient architectures. We demonstrate that our approach is competitive or superior to other state-of-the-art handcrafted networks. Furthermore, we demonstrate that the proposed NeuroLGP-SM approach is 25% more efficient in energy consumption, compared to a NeuroLGP variant that does not use surrogacy. Additionally, due to the unique encoding properties of

our NeuroLGP approach, we can easily analyse the internal structures of the architectures, giving greater insight into the favorable components of the discovered architectures.

ACKNOWLEDGEMENTS

This publication has emanated from research conducted with the financial support of Science Foundation Ireland under Grant number 18/CRT/6049. The author has applied a CC BY public copyright licence to any Author Accepted Manuscript version arising from this submission.

REFERENCES

- [1] M. Aswathy and M. Jagannath. An svm approach towards breast cancer classification from h&e-stained histopathology images based on integrated features. *Medical & biological engineering & computing*, 59(9):1773–1783, 2021.
- [2] J. A. Badejo, E. Adetiba, A. Akinrinmade, and M. B. Akanle. Medical image classification with hand-designed or machine-designed texture descriptors: a performance evaluation. In *Bioinformatics and Biomedical Engineering: 6th International Work-Conference, IWBBIO 2018, Granada, Spain, April 25–27, 2018, Proceedings, Part II 6*, pages 266–275. Springer, 2018.
- [3] Y. Benhammou, B. Achchab, F. Herrera, and S. Tabik. Breakhis based breast cancer automatic diagnosis using deep learning: Taxonomy, survey and insights. *Neurocomputing*, 375:9–24, 2020.
- [4] M. A. Bouhlel, N. Bartoli, A. Otsmane, and J. Morlier. Improving kriging surrogates of high-dimensional design models by partial least squares dimension reduction. *Structural and Multidisciplinary Optimization*, 53:935–952, 2016.
- [5] M. Brameier and W. Banzhaf. *Linear genetic programming*, volume 1. Springer, 2007.
- [6] N. V. Chawla, K. W. Bowyer, L. O. Hall, and W. P. Kegelmeyer. Smote: synthetic minority over-sampling technique. *Journal of artificial intelligence research*, 16:321–357, 2002.
- [7] K. Das, S. Conjeti, A. G. Roy, J. Chatterjee, and D. Sheet. Multiple instance learning of deep convolutional neural networks for breast histopathology whole slide classification. In *2018 IEEE 15th International Symposium on Biomedical Imaging (ISBI 2018)*, pages 578–581. IEEE, 2018.
- [8] S. Deng, Z. Lv, E. Galván, and Y. Sun. Evolutionary neural architecture search for facial expression recognition. *IEEE Transactions on Emerging Topics in Computational Intelligence*, 7(5):1405–1419, 2023.
- [9] S. Deng, Y. Sun, and E. Galvan. Neural architecture search using genetic algorithm for facial expression recognition. In *Proceedings of the Genetic and Evolutionary Computation Conference Companion, GECCO '22*, page 423–426, New York, NY, USA, 2022. Association for Computing Machinery.
- [10] A. E. Eiben and J. E. Smith. *Introduction to Evolutionary Computing*. Springer Verlag, 2003.
- [11] E. Galván and P. Mooney. Neuroevolution in deep neural networks: Current trends and future challenges. *IEEE Transactions on Artificial Intelligence*, 2:476–493, 2021.
- [12] E. Galván and M. Schoenauer. Promoting semantic diversity in multi-objective genetic programming. In A. Auger and T. Stützle, editors, *Proceedings of the Genetic and Evolutionary Computation Conference, GECCO 2019, Prague, Czech Republic, July 13–17, 2019*, pages 1021–1029. ACM, 2019.
- [13] E. Galván and F. Stapleton. Semantic-based distance approaches in multi-objective genetic programming. In *2020 IEEE Symposium Series on Computational Intelligence (SSCI)*, pages 149–156. IEEE, 2020.
- [14] E. Galván and F. Stapleton. Evolutionary multi-objective optimisation in neurotrajectory prediction. *Applied Soft Computing*, 146:110693, 2023.
- [15] E. Galván, L. Trujillo, and F. Stapleton. Semantics in multi-objective genetic programming. *Applied Soft Computing*, 115:108143, 2022.
- [16] I. Gonçalves, S. Silva, and C. M. Fonseca. Semantic learning machine: a feedforward neural network construction algorithm inspired by geometric semantic genetic programming. In *Progress in Artificial Intelligence: 17th Portuguese Conference on Artificial Intelligence, EPIA 2015, Coimbra, Portugal, September 8–11, 2015. Proceedings 17*, pages 280–285. Springer, 2015.

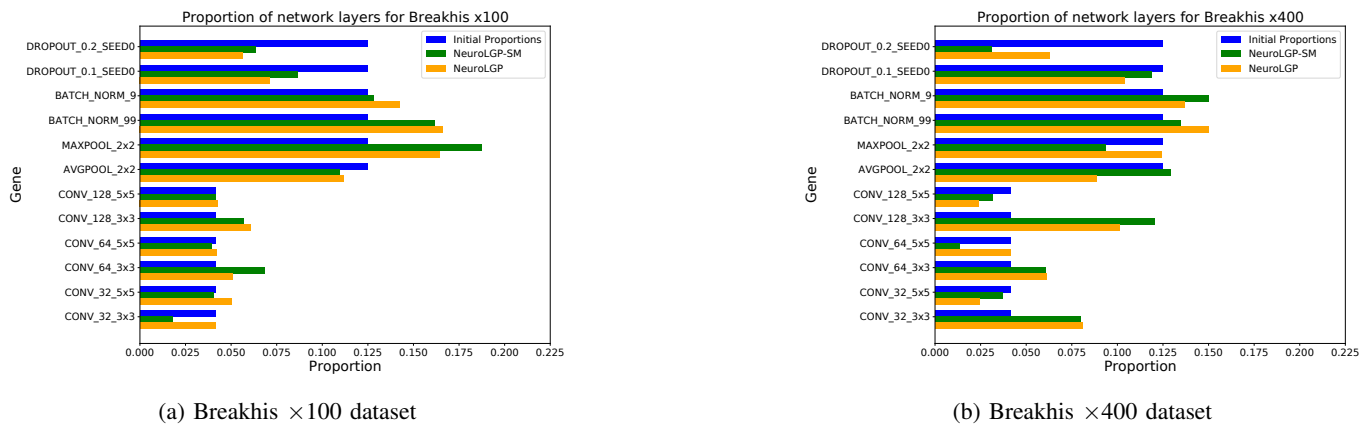


Fig. 6: Proportion of evolved network layers for initialisation (blue) and final generations for NeuroLGP-SM (green) and NeuroLGP (orange) for $\times 100$, and $\times 400$ datasets

- [17] B. Greenwood and T. McDonnell. Surrogate-assisted neuroevolution. In *Proceedings of the Genetic and Evolutionary Computation Conference*, pages 1048–1056, 2022.
- [18] V. Gupta and A. Bhavsar. An integrated multi-scale model for breast cancer histopathological image classification with joint colour-texture features. In *Computer Analysis of Images and Patterns: 17th International Conference, CAIP 2017, Ystad, Sweden, August 22-24, 2017, Proceedings, Part II 17*, pages 354–366. Springer, 2017.
- [19] A. Hagg, M. Zaefferer, J. Stork, and A. Gaier. Prediction of neural network performance by phenotypic modeling. In *Proceedings of the Genetic and Evolutionary Computation Conference Companion*, pages 1576–1582, 2019.
- [20] Y. Jin. Surrogate-assisted evolutionary computation: Recent advances and future challenges. *Swarm and Evolutionary Computation*, 1(2):61–70, 2011.
- [21] D. R. Jones, M. Schonlau, and W. J. Welch. Efficient global optimization of expensive black-box functions. *Journal of Global optimization*, 13:455–492, 1998.
- [22] R. Karthiga and K. Narasimhan. Automated diagnosis of breast cancer using wavelet based entropy features. In *2018 Second international conference on electronics, communication and aerospace technology (ICECA)*, pages 274–279. IEEE, 2018.
- [23] K. Kumar and A. C. S. Rao. Breast cancer classification of image using convolutional neural network. In *2018 4th International Conference on Recent Advances in Information Technology (RAIT)*, pages 1–6. IEEE, 2018.
- [24] L. Lannelongue, J. Grealey, and M. Inouye. Green algorithms: quantifying the carbon footprint of computation. *Advanced science*, 8(12):2100707, 2021.
- [25] Y. LeCun, Y. Bengio, and G. Hinton. Deep learning. *Nature*, 521(7553):436–444, 2015.
- [26] G. Menghani. Efficient deep learning: A survey on making deep learning models smaller, faster, and better. *ACM Computing Surveys*, 55(12):1–37, 2023.
- [27] A.-A. Nahid and Y. Kong. Histopathological breast-image classification using local and frequency domains by convolutional neural network. *Information*, 9(1):19, 2018.
- [28] A.-A. Nahid, M. A. Mehrabi, Y. Kong, et al. Histopathological breast cancer image classification by deep neural network techniques guided by local clustering. *BioMed research international*, 2018, 2018.
- [29] A.-A. Nahid, A. Mikaelian, and Y. Kong. Histopathological breast-image classification with restricted boltzmann machine along with backpropagation. *Biomedical Research*, 29(10):2068–2077, 2018.
- [30] S. Park and N. Kwak. Analysis on the dropout effect in convolutional neural networks. In *Computer Vision-ACCV 2016: 13th Asian Conference on Computer Vision, Taipei, Taiwan, November 20-24, 2016, Revised Selected Papers, Part II 13*, pages 189–204. Springer, 2017.
- [31] T. P. Pawlak, B. Wieloch, and K. Krawiec. Semantic backpropagation for designing search operators in genetic programming. *IEEE Transactions on Evolutionary Computation*, 19(3):326–340, June 2015.
- [32] S. Pratihier and S. Chatteraj. Diving deep onto discriminative ensemble of histological hashing & class-specific manifold learning for multi-class breast carcinoma taxonomy. In *ICASSP 2019-2019 IEEE International Conference on Acoustics, Speech and Signal Processing (ICASSP)*, pages 1025–1029. IEEE, 2019.
- [33] F. J. Santos, I. Gonçalves, and M. Castelli. Neuroevolution with box mutation: An adaptive and modular framework for evolving deep neural networks. *Applied Soft Computing*, page 110767, 2023.
- [34] M. Sharma, R. Singh, and M. Bhattacharya. Classification of breast tumors as benign and malignant using textural feature descriptor. In *2017 IEEE international conference on bioinformatics and biomedicine (bibm)*, pages 1110–1113. IEEE, 2017.
- [35] F. A. Spanhol, L. S. Oliveira, C. Petitjean, and L. Heutte. Breast cancer histopathological image classification using convolutional neural networks. In *2016 international joint conference on neural networks (IJCNN)*, pages 2560–2567. IEEE, 2016.
- [36] F. Stapleton, B. Cody-Kenny, and E. Galván. Neurolgp-sm: A surrogate-assisted neuroevolution approach using linear genetic programming. In *International Conference on Optimization and Learning (OLA)*, 2024.
- [37] F. Stapleton and E. Galván. Semantic neighborhood ordering in multi-objective genetic programming based on decomposition. In *2021 IEEE Congress on Evolutionary Computation (CEC)*, pages 580–587. IEEE, 2021.
- [38] F. Stapleton and E. Galvan. Initial steps towards tackling high-dimensional surrogate modeling for neuroevolution using kriging partial least squares. In *Proceedings of the Companion Conference on Genetic and Evolutionary Computation, GECCO '23 Companion*, page 83–84, New York, NY, USA, 2023. Association for Computing Machinery.
- [39] F. Stapleton, E. Galván, G. Sistu, and S. Yogamani. Neuroevolutionary multi-objective approaches to trajectory prediction in autonomous vehicles. In *Proceedings of the Genetic and Evolutionary Computation Conference Companion*, GECCO '22, page 675–678, New York, NY, USA, 2022. Association for Computing Machinery.
- [40] J. Stork, M. Zaefferer, and T. Bartz-Beielstein. Improving neuroevolution efficiency by surrogate model-based optimization with phenotypic distance kernels. In *International Conference on the Applications of Evolutionary Computation (Part of EvoStar)*, pages 504–519. Springer, 2019.
- [41] Y. Sun, H. Wang, B. Xue, Y. Jin, G. G. Yen, and M. Zhang. Surrogate-assisted evolutionary deep learning using an end-to-end random forest-based performance predictor. *IEEE Transactions on Evolutionary Computation*, 24(2):350–364, 2020.
- [42] Y. Sun, B. Xue, M. Zhang, and G. G. Yen. Evolving deep convolutional neural networks for image classification. *IEEE Transactions on Evolutionary Computation*, 24(2):394–407, 2019.
- [43] K. Swersky, J. Snoek, and R. P. Adams. Freeze-thaw bayesian optimization. *arXiv preprint arXiv:1406.3896*, 2014.
- [44] B. Zoph and Q. V. Le. Neural architecture search with reinforcement learning. *CoRR*, abs/1611.01578, 2016.